7

Optimal Design of the Tyre-Suspension System of a Racing Car

A racing car should be designed to improve the performance of the driver–vehicle system. Unfortunately, at present no readily exploitable driver models seem to be available. So the optimisation of a racing car refers mainly to the car itself. Contemporary tuning of both tyre characteristics and suspesnion system is of crucial importance. One of the main technical challenges is to achieve maximum cornering speed while balancing tyre forces at front and rear axles, improving handling ability.

In order to design effectively a racing car, one may be requested to tune the entire set of design variables related to tyres, aerodynamics and chassis characteristic (stiffness, damping and kinematics of the suspension system). This is not a straightforward problem especially if one exploits very sophisticated models defined by many parameters. In fact, when many design variables have to be changed, their tuning has to be performed by using adequate optimisation theories (see Sect. 2.10) and related software tools. Traditionally, the process of tuning the car has been performed by a trial-and-error approach based on professional drivers' feedback. A sensitivity analysis [32] is of limited help to the designer if the number of design variables is high.

A more rational approach compared to a trial-and-error procedure is desirable. Multi-objective optimisation is the most effective way for optimising complex systems, i.e. systems, which are described by many design variables and which perform many functions [149] (see Chap. 3).

In the literature, several papers [93,94,141] have dealt with the problem of the optimisation of a car suspension system by means of the multi-objective approach.

This chapter, derived from [161], presents a procedure that can be used for the integrated design (tuning) of tyres and suspensions of a racing car.

A complete model of a racing car has been developed and implemented through a series of programming codes. Elasto-kinematics of the suspension system, powertrain and braking systems have been described in detail. Tyre characteristics have been identified and implemented by means of

Pacejka's Magic Formulæ. The aerodynamic characteristics of the body have been measured in wind tunnel and included into the model.

A number of ground tests, according to the ISO standards, have been performed to validate the vehicle model. The main dynamic responses of the car have been recorded and compared with the computed responses, with fully satisfactory results.

Proper objective functions have been defined after a subjective–objective correlation analysis. Many different driving situations (steady-state, J-turn, lane-change, power on–off while steering, braking on a bend, passing over a kerb while steering) have been considered. By means of a multi-objective (Sect. 2.10) approach, 26 objective functions, defined after a subjective–objective correlation analysis, have been optimised by changing 18 design variables related with the suspension system and the tyre characteristics. A global approximation model (see Sect. 4) has been followed (the original physical car model has been substituted by another purely numerical model), allowing fast optimisations.

7.1 System Model

A vehicle model, divided into modules, has been constructed on the basis of one presented in [93]. Each module represents a vehicle sub-system (Fig. 7.1) which interacts with the other sub-systems by means of input/output variables.

The result is an 18 d.o.f.s model that simulates satisfactorily the actual vehicle dynamic behaviour (Table 7.2).

7.1.1 Vehicle Model

Car chassis is considered as a rigid body. Tyre forces are transmitted to the front and rear axle modules respectively (Fig. 7.1). Front and rear axle modules apply two resultant forces and two resultant torques to points A and B respectively (Fig. 7.1). Aerodynamic forces are modeled assuming front lift, rear lift and drag coefficients depending on front and rear vertical position of points A and B with respect to the ground.

Front and rear independent suspension systems have a double wishbone layout, different layouts can be easily considered referring to available libraries [158]. Shock absorbers are modeled as non-linear components; forces transmitted by the shock absorber are function of the deformation speed. Non-linearity due to bump-stop characteristics has been included.

The torque-speed characteristic of the differential has been derived experimentally and accurately modeled. The braking system is modeled by considering the different distribution of braking force between front and rear axle.

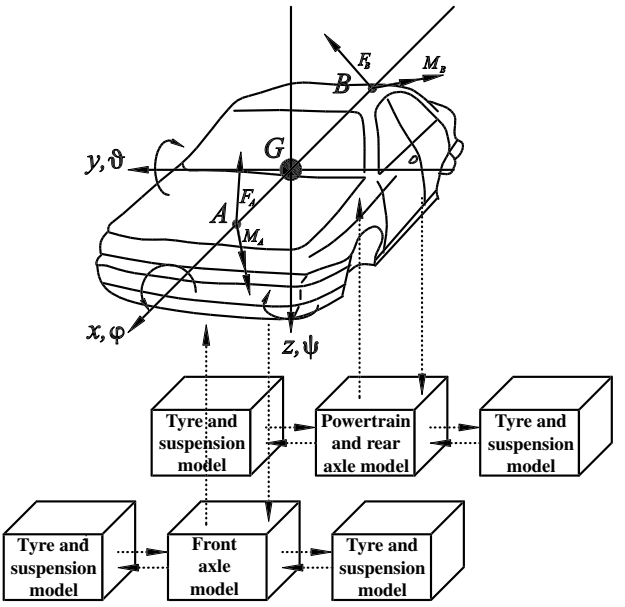

Fig. 7.1. Vehicle model. Dotted arrows refer to input–output variables describing the dynamics of each module

7.1.2 Tyre Model

A model that allows to estimate tyre forces with a good accuracy has been implemented on the basis of *Pacejka's Magic Formulæ* [10, 110, 194–196]. Tyre characteristics have been measured on a flat-track machine [208]. Experimental measurements have been used to identify Pacejka's model coefficients by applying the procedure reported in [187]. The model enables to simulate tyre behaviour at high slip angles and high level of longitudinal slip. The transient tyre behaviour is given by

$$\chi\left(F_z\right)\frac{dF_y}{dt} + v_w\,F_y = v_w\,F_{y,stat}\left(\alpha, F_z, \gamma\right) \tag{7.1}$$

This formulation allows to include the *relaxation length* effect. Combined effects of longitudinal and lateral slip have been considered [225].

Four d.o.f.s are used to simulate vertical motions of unsprung masses and four d.o.f.s refer to the rolling of the wheels.

7.1.3 Validation

Results given by simulations have been compared with track test measures on a test vehicle. The test vehicle is equipped with a data acquisition computer, wheel speed sensors, throttle position sensor, gear position sensor, brake circuit pressure sensors, steering wheel angle sensor, vehicle body

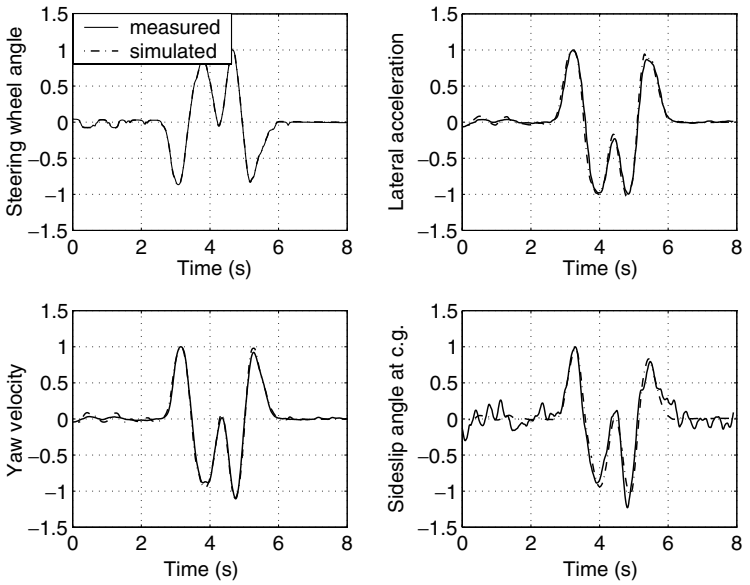

Fig. 7.2. Severe lane-change manoeuvre, numerical and experimental data. The measured steering wheel angle is used as input for the simulation code (throttle and selected gear are constant during the manoeuvre). Non-dimensional values on the y-axes ($y_{actual}/y_{max,measured}$)

accelerometers and gyroscopes, optical vector speed sensor. Measurements are matched directly with computed data. A parameter identification procedure is not needed. Comparisons considering a severe lane-change manoeuvre (ISO 3888) are shown in Fig. 7.2. The agreement is good. A test run on track is shown in Fig. 7.3. Again the model proves to represent fairly the dynamic behaviour of the car under consideration.

7.2 Design Variables

Eighteen design variables have been considered for the optimisation process. Design variables are related to suspension springs, anti-roll bars, hydraulic dampers, static toe angles, static camber angles and tyre characteristics. These design variables have been chosen as they are reputed to influence the behaviour of the vehicle taken under consideration. Moreover, these design variables can be easily modified on the considered vehicle.

Three types of optimisation strategies have been performed:

(1) Changing the stiffness of the front and rear suspension springs, the front anti-roll bar and the static toe and camber angles of front and rear wheels according to a grid (see Sect. 3.4.2).

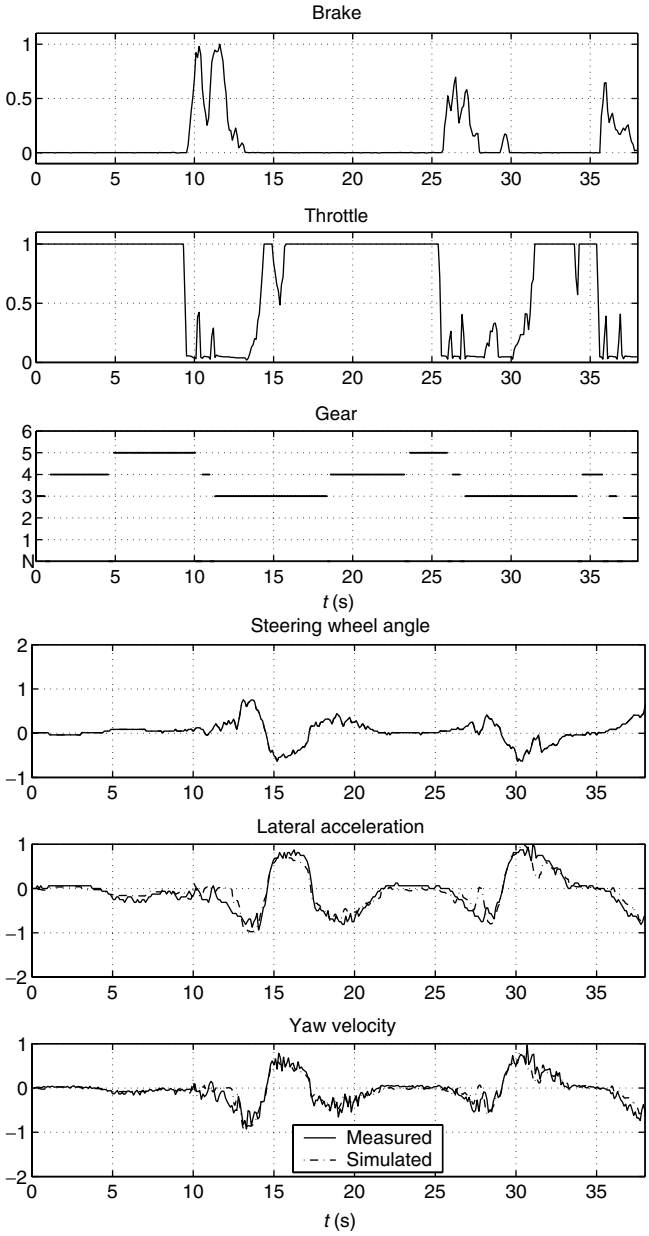

Fig. 7.3. Test run on track. The measured steering wheel angle, throttle position, gear and brake position are used as inputs for the simulation code. Non-dimensional values on y-axes ($y_{actual}/y_{max,measured}$). The only relevant discrepancy between measured and computed data (at $t = 10$–$13\,\mathrm{s}$) is due to the hitting of a kerb

(2) Changing suspension characteristics (stiffness, damping, toe and camber) by varying design variables continuously within specified ranges.
(3) Changing tyre and suspension characteristics by varying design variables continuously within specified ranges.

The design variables variations are shown in Table 7.1.

Table 7.1. Variation of the design variables values with respect to the reference vehicle

Design variable	1st optimisation	2nd optimisation	3rd optimisation
$k_{s,F}$	-20%, ref.	$[-50\%, +10\%]$	$[-50\%, +10\%]$
$k_{s,R}$	-20%, ref.	$[-60\%, +10\%]$	$[-60\%, +10\%]$
$k_{r,F}$	-40%, ref.	$[-80\%, +60\%]$	$[-80\%, +60\%]$
$k_{r,R}$	Ref.	$[-80\%, +100\%]$	$[-80\%, +100\%]$
$r_{b,l,F}$	Ref.	$[-60\%, +90\%]$	$[-60\%, +90\%]$
$r_{b,l,R}$	Ref.	$[-60\%, +90\%]$	$[-60\%, +90\%]$
$r_{r,l,F}$	Ref.	$[-50\%, +50\%]$	$[-50\%, +50\%]$
$r_{r,l,R}$	Ref.	$[-50\%, +50\%]$	$[-50\%, +50\%]$
$\delta_{st,F}$	-130%, -65%, ref., $+65\%$, $+130\%$	$[-130\%, +130\%]$	$[-130\%, +130\%]$
$\delta_{st,R}$	-80%, -40%, ref., $+40\%$, $+80\%$	$[-80\%, +80\%]$	$[-80\%, +80\%]$
$\gamma_{st,F}$	-30%, -15%, ref., $+15\%$, $+30\%$	$[-30\%, +30\%]$	$[-30\%, +30\%]$
$\gamma_{st,R}$	-30%, -15%, ref., $+15\%$, $+30\%$	$[-30\%, +30\%]$	$[-30\%, +30\%]$
$p_{1,F}$	Ref.	Ref.	$[-15\%, +15\%]$
$p_{1,R}$	Ref.	Ref.	$[-15\%, +15\%]$
$p_{2,F}$	Ref.	Ref.	$[-15\%, +15\%]$
$p_{2,R}$	Ref.	Ref.	$[-15\%, +15\%]$
C_F	Ref.	Ref.	$[-15\%, +15\%]$
C_R	Ref.	Ref.	$[-15\%, +15\%]$

Three optimisation strategies are considered. Design variables referring to the first optimisation have only discrete values ('ref.' means 'reference value')

7.2.1 Suspension System

Twelve design variables (system's model parameters) are tuned (Table 7.1) referring to

– the suspension spring characteristic (front and rear);
– the anti-roll bar characteristic (front and rear);
– the characteristic of the hydraulic dampers (front and rear) (four design variables);
– the suspension geometry (front and rear) (four design variables)

Table 7.2. List of main parameters values used in the presented simulations

l_F	Distance ofbody centre of mass from the front axle	1.497 m
$l_F + l_R$	Wheelbase	2.568 m
c_F/c_R	Half track front/rear	0.85 m/0.80 m
h	Height of the vehicle body centre of mass	0.428 m
m	Vehicle body mass	1,020 kg
m_F/m_R	Wheel mass (right + left) front and rear	80 kg/100 kg
$J_x/J_y/J_z$	Moments of inertia of the vehicle body about x-, y-, z-axis	330 kgm^2, 1,600 kgm^2, 1,800 kgm^2
C_dS	Drag	0.71 m^2
ET_{max}	Engine maximum torque	400 Nm@6,000 rpm
$C_{\alpha,F}/C_{\alpha,R}$	Cornering stiffness front/rear tyres	121,000 N/rad, 182,000 N/rad

Suspension Springs

Front and rear stiffness of the suspension springs, have been varied. The values of the design variables during the optimisation process are shown in Table 7.1.

Anti-roll Bars

Stiffness of front and rear anti-roll bar have been varied. These design variables during optimisation process are shown in Table 7.1.

Hydraulic Dampers

The force transmitted as a function of damper speed is modeled as shown in Fig. 7.4. Forces are given by

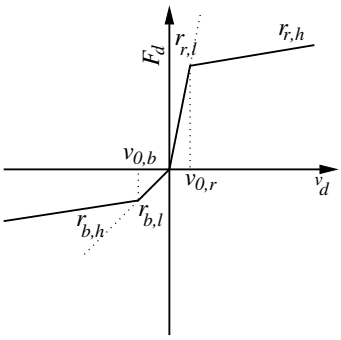

Fig. 7.4. Non-linear hydraulic damper characteristic, force vs. damper speed

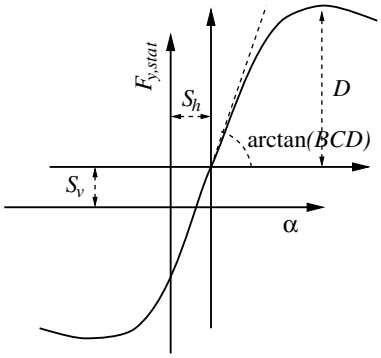

Fig. 7.5. A typical tyre characteristic (see Eq. (7.3))

$$\begin{cases} F_d = r_{r,h}\,(v_d - v_{0,r}) + r_{r,l}\,v_{0,r} & v_d > v_{0,r} \\ F_d = r_{r,l}\,v_d & v_d > 0,\ v_d \le v_{0,r} \\ F_d = r_{b,l}\,v_d & v_d > v_{0,b},\ v_d \le 0 \\ F_d = r_{b,h}\,(v_d - v_{0,b}) + r_{b,l}\,v_{0,b} & v_d \le v_{0,b} \end{cases} \tag{7.2}$$

Four design variables $r_{b,l}$, $r_{r,l}$, $r_{b,h}$, $r_{r,h}$ describe the shock absorber characteristic [87]. Velocities $v_{0,b}$ and $v_{0,r}$ are kept fixed, only $r_{b,l}$ and $r_{r,l}$ are varied during the optimisation process. Values assumed by these design variables are shown in Table 7.1.

Suspension Geometry

Suspension geometry is optimised by changing the static values of camber and toe angles. Values assumed by these design variables are shown in Table 7.1.

7.2.2 Tyre Characteristic

For pure lateral slip *Pacejka's Magic Formulæ* express the side force $F_{y,stat}$ as a function of the side slip angle α. The general form for a given value of vertical load and camber reads (Fig. 7.5)

$$F_{y,stat} = D \sin\{C \arctan[B(\alpha + S_h) - E\,(B(\alpha + S_h) - \arctan\,(B(\alpha + S_h)))]\} + S_v \tag{7.3}$$

Figure 7.5 shows the meaning of coefficients BCD and D for a typical tyre force characteristic. Coefficient D represents the peak value of the lateral force (if $S_v = 0$) and the product BCD corresponds to slope at the origin of the curve (if $S_h = 0$ and $S_v = 0$). The factor C controls the domain of the sine function in Eq. (7.3), and determines the shape of the resulting curve. The function of the cornering stiffness BCD reads

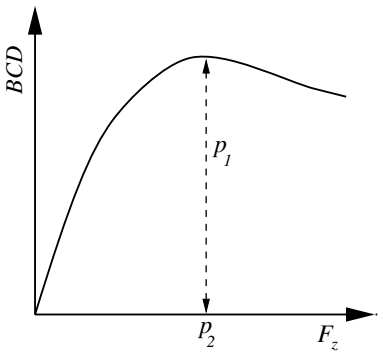

Fig. 7.6. Cornering stiffness as a function of vertical load according to expression (7.4) at camber zero

$$BCD = p_1 \sin\left[2\arctan\left(\frac{F_z}{p_2}\right)\right](1 - p_3\,|\gamma|) \tag{7.4}$$

For zero camber, the cornering stiffness has a maximum p_1 at $F_z = p_2$. Figure 7.6 shows the relationship given in (7.4).

C, p_1 and p_2 are chosen as design variables their variations are reported in Table 7.1.

7.3 Running Situations and Objective Functions

The vehicle–driver system and the external environment constitute a complex closed-loop system. The evaluation of the handling behaviour is made difficult by the human–vehicle interaction. Only a limited number of standard manoeuvres and running conditions have been defined by ISO and generally no evaluation criteria are given. In the following application a total number of six running situations (26 objective functions) are at first introduced.

7.3.1 Steady-state Turning

The simulation of the steady-state turning manoeuvre is based on ISO 4138 standard. The vehicle has to be driven on a known circular path at different speeds. This manoeuvre can be used to assess the tendency of the vehicle to understeer–oversteer by computing *understeer/oversteer gradient*:

$$\frac{d\delta}{da_c} \tag{7.5}$$

This parameter is strictly related to driver perception. Oversteering vehicles at high levels of lateral acceleration will be discarded during the search procedure. Considered objective functions are reported in Table 7.3.

Table 7.3. Optimisation scheme

Symbol	Objective function	Goal
Steady-state turning		
$a_{c,50m}$	Maximum a_c ($\rho = 50\,\mathrm{m}$)	Maximise
$\beta_{1.3\,g,50m}$	β ($a_c = 13\,\mathrm{m/s^2}$, $\rho = 50$ m)	Minimise
$P_{1.3\,g,50m}$	Power required ($a_c = 13\,\mathrm{m/s^2}$, $\rho = 50\,\mathrm{m}$)	Minimise
$a_{c,120m}$	Maximum a_c ($\rho = 120\,\mathrm{m}$)	Maximise
$\beta_{1.3\,g,120m}$	β ($a_c = 13\,\mathrm{m/s^2}$, $\rho = 120\,\mathrm{m}$)	Minimise
$P_{1.3\,g,120m}$	Power required ($a_c = 13\,\mathrm{m/s^2}$, $\rho = 120\,\mathrm{m}$)	Minimise
J-turn		
$t_{\dot{\psi}}$	$\dot{\psi}$ peak response time	Minimise
$O_{\dot{\psi}}$	$\dot{\psi}$ overshoot	Minimise
$\dot{\psi}_{s,s}$	Steady-state $\dot{\psi}$	Maximise
t_β	β peak response time	Minimise
O_β	β overshoot	Minimise
β_{max}	Maximum β	Minimise
$\beta_{s,s}$	Steady-state β	Minimise
t_{a_c}	a_c peak response time	Minimise
O_{a_c}	a_c overshoot	Minimise
$a_{c,max}$	Maximum a_c	Maximise
$a_{c,s,s}$	Steady-state a_c	Maximise
$RMS(\dot{\beta})_{J\,turn}$	Root mean-square of $\dot{\beta}$	Minimise
y_{path}	deviation from straight path	Maximise
$t_{a_c} - t_{\dot{\psi}}$	time delay between a_c and $\dot{\psi}$	Minimise
TB	TB factor	Minimise
Power on–off		
$RMS(\dot{\beta})_{Pwr\,on-off}$	*Root mean-square of* $\dot{\beta}$	Minimise
Braking on a bend		
$F_{z,max,left}$	Minimum vertical load on left rear wheel	Maximise
$F_{z,max,right}$	Minimum vertical load on right rear wheel	Maximise
Passing on a kerb while steering		
$RMS(F_{z,f,left})$	Root mean-square of the front left wheel vertical load	Minimise
$RMS(F_{z,r,left})$	Root mean square of the right left wheel vertical load	Minimise

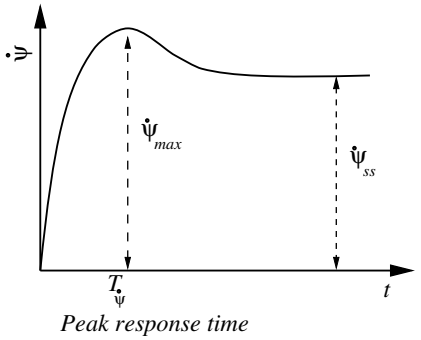

Fig. 7.7. Values for defining the peak response time and the overshoot with reference to yaw velocity response

7.3.2 J-Turn

The simulation of the J-turn manoeuvre (based on ISO 7401 standard with some minor adaptations due to the fact that a racing car is considered) provides information on transient vehicle response. The time histories of the centripetal acceleration, of the sideslip angle and of the yaw rate are considered as responses to a standard steering-wheel ramp input. The objective functions are the peak response time of the responses to a steering wheel step input and the overshoots of the responses (related to damping level of the system). In Fig. 7.7 a typical yaw velocity response to a steering step input is shown. Peak response time ($t_{\dot{\psi}}$) is highlighted. The expression of the overshoot is

$$O_{\dot{\psi}} = \frac{\dot{\psi}_{Max} - \dot{\psi}_{steady\ state}}{\dot{\psi}_{steady\ state}} \tag{7.6}$$

The peak response time and the overshoot for β and a_c are defined similarly as in (7.6). The TB factor [167] is an important objective function referring to a J-turn manoeuvre. TB is calculated as the product of the yaw velocity peak response time and the steady-state sideslip angle at the vehicle centre of gravity:

$$TB = t_{\dot{\psi}} \cdot \beta_{s,s} \tag{7.7}$$

A low value of the TB factor seems implying good vehicle handling characteristics. Objective functions for this manoeuvre are reported in Table 7.3.

7.3.3 Power On–Off while Steering

This manoeuvre is included in order to analyse the vehicle reactions to a power on–off input during turning. This type of input could excite undesirable

reactions that are perceived negatively by the driver. The vehicle runs into a bend in a steady-state condition at a high level of lateral acceleration and suddenly the throttle is fully opened (< 0.3 s), after 3 s it is fully released and then reopened (< 0.3 s). The steering-wheel angle is kept constant during the whole manoeuvre. Root mean square of $\dot{\beta}$ is the variable taken as a objective function during this manoeuvre (Table 7.3). This variable shows the tendency of the vehicle to oscillate around the centre of gravity.

7.3.4 Braking into a Bend

A typical braking manoeuvre before negotiating a bend is simulated. Load transfer in this running situation drives to unstability. This manoeuvre is composed by a sudden release of the throttle and subsequent full brake application. During the turning the brake is released gradually. The steer, brake and throttle inputs are shown in Fig. 7.8. The objective functions for this manoeuvre are reported in Table 7.3.

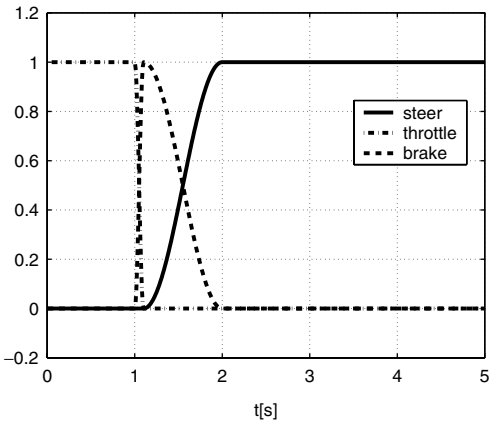

Fig. 7.8. Braking into a bend steer, brake and throttle inputs (non-dimensional values on y-axes (y_{actual}/y_{max}))

7.3.5 Passing over a Kerb While Steering

Passing over a kerb while steering provides information of both low-frequency and high-frequency vehicle responses. The obstacle is asymmetric and excites the roll motion of the vehicle body. The maximum height of the obstacle is 50 mm. The vertical shape of the kerb is shown in Fig. 7.9. The objective functions are indicated in Table 7.3.

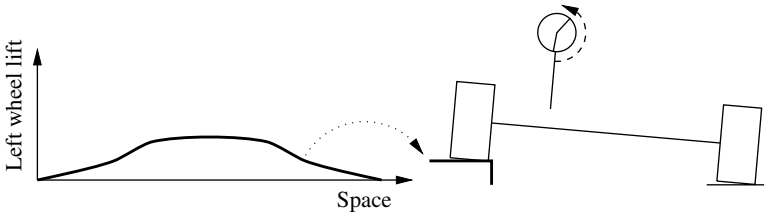

Fig. 7.9. Passing over a kerb

7.4 Search Method

The optimisation method [87,88] is based on two different mathematical models of the same car whose design variables have to be optimised. The first is a physical model, i.e. it is derived on the basis of a mechanical model strictly related to the vehicle system (the model is described in Sect. 7.1.1). The second model ('global approximation' see Chap. 4) is just a set of functions that are able to approximate many different relationships that exist between the design variables and the objective functions, describing the vehicle system responses.

The global approximation model has been constructed by means of an artificial neural network. Multi-layer perceptron neural networks have been used to approximate (within a very small computation time) complex non-linear functions with an arbitrary degree of accuracy [88, 113] (see Chap. 4). To avoid overtraining, a cross-validation procedure (see Chap. 4) [127] has been implemented.

7.4.1 Reduction of Objective Functions

N ($<10^3$) solutions have been analysed in order to reduce the number of objective functions that have to be taken into account. This has been done by using the 'Spearman rank correlation coefficient' (see Chap. 3) [182]. Some strongly correlated objective functions were found (even non-linear correlations were detected, Fig. 7.10), so the existence of redundancy was discovered (see Table 7.4) and the number of objective functions could be reduced [87, 182].

7.4.2 Pareto-optimal Solutions

The 'global approximation' model is used during the search procedure for the computation of the Pareto-optimal set (see Sect. 2.10).

The main advantage of multi-objective programming is that it provides a rational approach to decision making in the presence of conflicting criteria.

The global approximation allows a quick computation of the optimal sets of design variables, generally much faster than the computation by using the physical model.

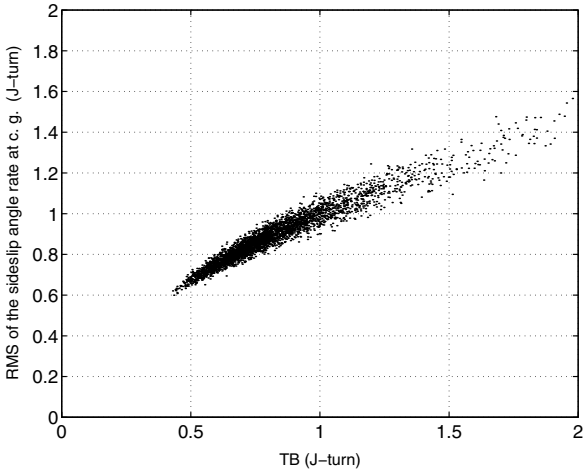

Fig. 7.10. Example of correlation between two objective functions in non-dimensional form. Spearman Rank Correlation Coefficient = 0.971

Table 7.4. Objective functions eliminated by using the Spearman rank correlation analysis

Eliminated objective function	Correlated objective function	r_s
$\beta_{1.3\,g,50\,m}$	$\beta_{1.3\,g,120\,m}$	0.997
$P_{1.3\,g,50\,m}$	$P_{1.3\,g,120\,m}$	0.996
$t_{\dot{\psi}}$	TB	0.926
t_{β}	TB	0.950
β_{max}	TB	0.964
$\beta_{s,s}$	TB	0.963
$a_{c,max}$	$\dot{\psi}_{s,s}$	0.947
$a_{c,s,s}$	$\dot{\psi}_{s,s}$	0.991
$RMS(\dot{\beta})_{Jturn}$	TB	0.971
y_{path}	$\dot{\psi}_{s,s}$	0.974
$F_{z,max,right}$	$F_{z,max,left}$	0.997

A large number ($>10^6$) of uniformly distributed solutions can be generated by the neural net approximation within a short time (see Chap. 4). Condition (2.11) can be checked and the Pareto-optimal solutions can be stored.

The designer can choose a preferred solution among those (and only those) belonging to the Pareto-optimal set.

7.5 Results

Two thousand uniformly distributed design variable vectors have been generated and used to compute the responses of the physical model.

By applying the procedure described in Sect. 7.4.1 only 15 objective functions were selected and considered for the subsequent optimisation. In fact they resulted fully representative of the 26 objective functions initially considered.

A multi-layer perceptron neural network has been trained approximating the 15 objective functions as a function of 18 design variables. The mean error of the trained neural network is less than 3%.The network architecture has two layers of 70 and 40 neurons respectively. The training set is composed of only 1,000 responses of the physical model out of the 1,200 generated. A number of candidate optimal solutions have been selected from the Pareto-optimal set.

Figures 7.11 and 7.12 show two projections of the Pareto-optimal set onto two planes. Data are reported in non-dimensional form. Improvements are obtained for all the objective functions.

A preferred solution has been chosen from the Pareto-optimal set and it has been denoted as *optimised car*. The results of the third optimisation (Table 7.1) are reported, because the improvements obtainable by varying a reduced set of design variables (first and second optimisation) were not fully satisfactory. The improvements with respect to the reference car are shown in Table 7.5.

The mean improvement (on all the 26 objective functions) is about 10%. The handling behaviour is significantly improved. The reference car does not seem belonging to the Pareto-optimal set. Comparisons between reference car and optimised car are shown in Figs. 7.13–7.15, referring to a J-turn manoeuvre, a steady-state turning manoeuvre and a power on–off while steering manoeuvre. Steady-state turning manoeuvres (Fig. 7.14) show higher level of centripetal acceleration that can be achieved by the optimised car with respect to the reference car. This is due to a better load transfer distribution between front and rear axles. Moreover, in this manoeuvre the sideslip angle is reduced because of the higher cornering stiffness of the rear tyres. The power required is reduced (up to 12% at the highest lateral acceleration) because the slippages of the optimised vehicle are less than the slippage of the reference vehicle. J-turn manoeuvre reveals (Fig. 7.13) a more damped motion of the optimised vehicle with respect the reference vehicle due to a different stiffness and damping distribution between front and rear axles. This is done by maintaining the TB factor at about the same level. The same damping effect holds for Power on–off manoeuvre (Fig. 7.15). $F_{z,max,left}$ is improved because $r_{b,l,F}$ is augmented and $r_{r,l,R}$ is reduced. $RMS(F_{z,r,left})$ is less because damping of the rear shock absorbers are greatly decreased, being $k_{s,R}$ equal.

7.5.1 Comparison of the Performances of Global Approximation Methods

Three approximation methods, polynomial approximation, RBFNN and MLPNN (see Chap. 4) are trained using a sample of 2,023 point obtained from a $(t, 16)$-sequence in base 17 (see Sect. 3.4.2). The design variables and the objective functions are normalised before the application of the methods. The set of 2,023 design points is split into two set $\mathcal{D}(n_D)$ and $\mathcal{V}(n_V)$ to train

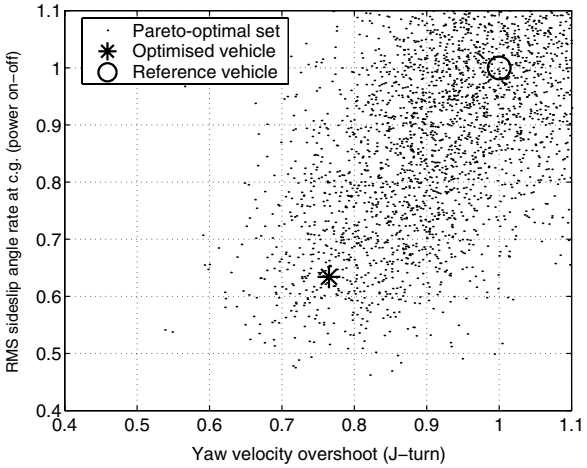

Fig. 7.11. Pareto-optimal set projection onto $(RMS(\dot{\beta})_{Pwr\,on-off}, O_{\dot{\psi}})$ plane. Data are plotted in non-dimensional form

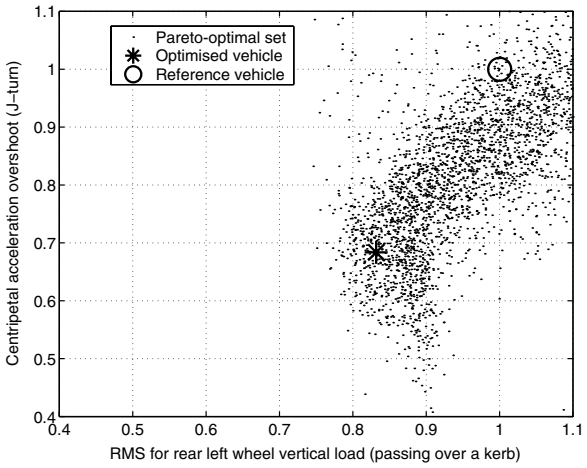

Fig. 7.12. Pareto-optimal set projection onto $(O_{a_c}, RMS(F_{z,r,left}))$ plane. Data are plotted in non-dimensional form

Table 7.5. Design variables and objective functions of a preferred car denoted as 'optimised vehicle'

Design variable	Variation with respect to the reference car (%)
$k_{s,F}$	−10
$k_{s,R}$	0
$k_{r,F}$	−15
$k_{r,R}$	+73
$r_{b,l,F}$	+83
$r_{b,l,R}$	−38
$r_{r,l,F}$	−18
$r_{r,l,R}$	−49
$\delta_{st,F}$	−43
$\delta_{st,R}$	+31
$\gamma_{st,F}$	+9
$\gamma_{st,R}$	+18
$p_{1,F}$	+1
$p_{1,R}$	+8
$p_{2,F}$	+12
$p_{2,R}$	−2
C_F	+3
C_R	+10

Objective function index	Improvement with respect to the reference car (%)
$a_{c,\,50\,m}$	3
$a_{c,\,120\,m}$	3
$\beta_{1.3\,g,120\,m}$	6
$P_{1.3\,g,120\,m}$	2
$O_{\dot{\psi}}$	24
$\dot{\psi}_{s,s}$	1
O_{β}	16
t_{a_c}	0
O_{a_c}	32
$t_{a_c} - t_{\dot{\psi}}$	1
TB	0
$RMS(\dot{\beta})_{Pwr\,on-off}$	36
$F_{z,max,left}$	15
$RMS(F_{z,f,left})$	0
$RMS(F_{z,r,left})$	16

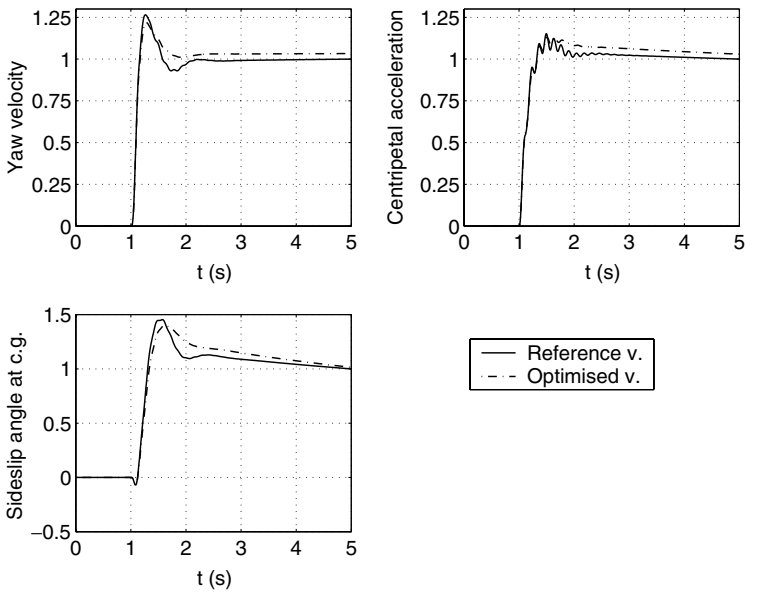

Fig. 7.13. J-turn manoeuvre. Comparisons between reference and optimised vehicle. (Data are normalised with respect to the steady-state values of the reference vehicle)

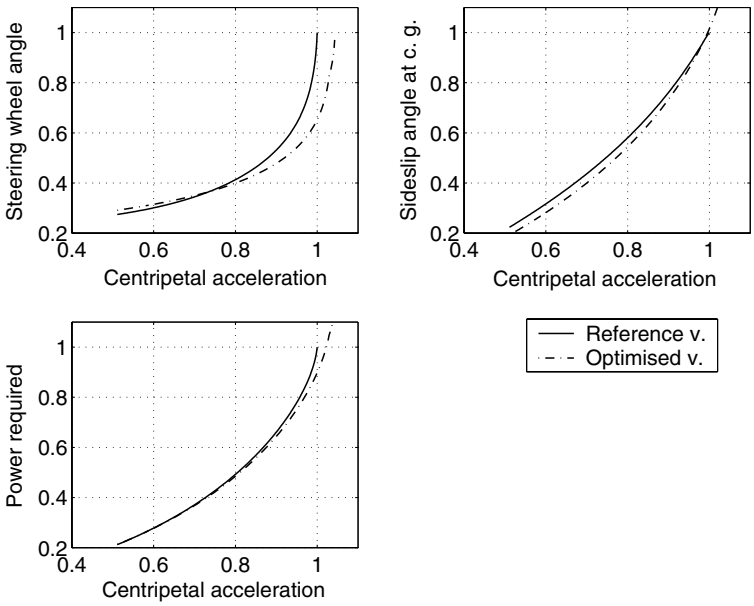

Fig. 7.14. Steady-state turning. Comparisons between reference and optimised vehicle. (Data are normalised with respect to the maximum values of the reference vehicle).

the multi-layer perceptron neural network. The $\mathcal{D}(N_D)$ is the training set and $n_D = 1{,}734$, $\mathcal{V}(N_V)$ is the validation set used for cross-validation (see Sect. 4.6.1) and $N_V = 289$. The models are tested on a set $\mathcal{T}(N_T)$ of $N_T = 14{,}739$ points.

Different types of error estimators are considered.

1. The *mean relative error* is defined by

$$\Delta_j = \frac{1}{N_T} \sum_{i=1}^{N_T} \frac{|\hat{y}_{ij} - y_{ij}|}{|y_{ij}|} \tag{7.8}$$

   lower Δ_j refers to a good approximation.
2. The *normalised standard deviation* is defined by

$$\Sigma_j = \sqrt{\frac{\sum_{i=1}^{N_T} \left(\hat{y}_{ij} - y_{ij}\right)^2}{\sum_{i=1}^{N_T} \left(y_{ij} - \bar{\bar{y}}_j\right)^2}} \tag{7.9}$$

   where $\bar{\bar{y}}_j = \frac{1}{N_T} \sum_{i=1}^{N_T} y_{ij}$. Lower Σ_j refers to good a approximation.
3. The *correlation coefficient* between the estimated $\hat{y}_{ij}$ output and the test output y_{ij}

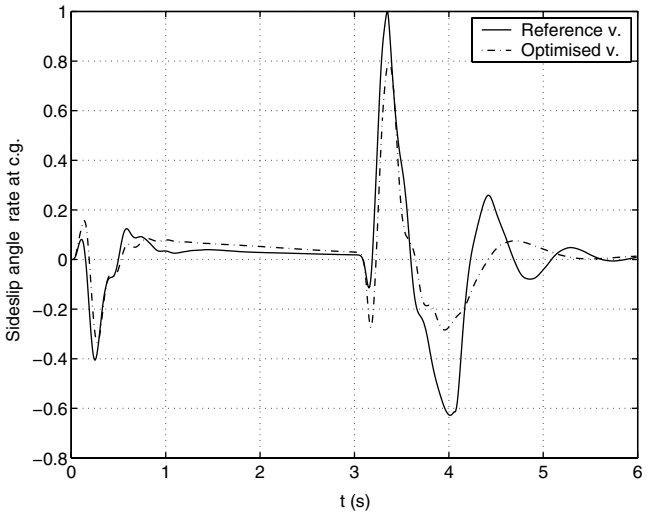

Fig. 7.15. Power on–off manoeuvre (see Sect. 7.3.3). Comparisons between reference and optimised vehicle. (Data are normalised with respect to the maximum values of the reference vehicle)

$$R_j = \frac{\sum_{i=1}^{N_T} \left(\hat{y}_{ij} - \hat{\bar{y}}_j\right)\left(y_{ij} - \bar{y}_j\right)}{\sqrt{\sum_{i=1}^{N_T} \left(\hat{y}_{ij} - \hat{\bar{y}}_j\right)^2 \sum_{i=1}^{N_T} \left(y_{ij} - \bar{y}_j\right)^2}} \tag{7.10}$$

where $\hat{\bar{y}}_j = \frac{1}{N_T} \sum_{i=1}^{N_T} \hat{y}_{ij}$. Value of R_j closer to 1 refers to a good approximation.

Four approximation models have been compared in terms of accuracy:

1. linear approximation (Sect. 4.3.1). The number r of function employed is 17 for every objective function;
2. polynomial quadratic approximation (Sect. 4.3.1). The number r of function employed is 153 for every objective function;
3. radial basis function neural network regularised and trained using regression trees (Sect. 4.6.2) with Gaussian basis functions. N_{min} is 2 (N_{min} is the unique parameter to be set by the user and refers to the number of points that are considered to stop the generation of the regression tree);
4. Radial basis function neural network regularised and trained using regression trees (Sect. 4.6.2) with thin plate spline basis functions. N_{min} is 2;
5. Multi-layer perceptron neural network (MLPNN) trained using early stopping (Sect. 4.6.1). The final network architecture is composed by two hidden layers with 98 and 105 neurons.

It is important to notice that the approximations model based on NN needs to be designed and trained properly. This procedure is time-consuming and the

generation of the approximation model requires more time than other methods (see Table 7.11). Actually, a trial-and-error procedure has to be completed for the setting of the number of neurons and hidden layers. In contrast to the complex setting of parameters referring to the architecture of MLPNN, the RBFNN requires to set only one parameter: N_{min} that defines the regression tree structure (see Sect. 4.6.2).

By inspection of Table 7.6, one may easily notice that the MLPNN is superior with respect to other methods for approximation purposes (see mean Δ_j values). The same could be stated for the other test criteria (Eqs. (7.9) and (7.10); Tables 7.7 and 7.8). In these cases RBFNN methods show performance (both with Gaussian basis functions and with thin plate spline basis functions) close to MLPNN, confirming the results presented in [229]. The results (Tables 7.6–7.8) show also that the linear approximation model is inadequate for the problem under consideration. The quadratic approximation model may be good for the approximation of some objective functions but for other objective functions the approximation is insufficient (see maximum values in Tables 7.6– and minimum values in Table 7.8)[1].

Table 7.6. Relative errors

Method	1(%)	2(%)
Linear	5.67	27.92
Quadratic	4.16	26.52
RBFNN gaussian	2.87	9.49
RBFNN thin plate spline	2.91	9.38
MLPNN	2.44	15.46

(1) Mean $\triangle_j$ over all the considered objective functions.
(2) Maximum $\triangle_j$ over all the objective functions

Table 7.7. Normalised standard deviation

Method	1	2
Linear	0.270	0.482
Quadratic	0.175	0.402
RBFNN gaussian	0.156	0.385
RBFNN thin plate spline	0.158	0.386
MLPNN	0.132	0.298

(1) Mean Σ_j over all the considered objective functions.
(2) Maximum Σ_j over all the objective functions

[1]We must emphasise that this is only the time needed for a single training of the MLPNN; MLPNN needs multiple training to determine the optimal network architecture

Table 7.8. Correlation coefficient between estimated $\hat{y}$ and real y of different methods

Method	1	2
Linear	0.898	0.732
Quadratic	0.948	0.809
RBFNN gaussian	0.971	0.877
RBFNN thin plate spline	0.970	0.881
MLPNN	0.980	0.960

(1) Mean R_j over all the considered objective functions.
(2) Minimum R_j over all the objective functions

Table 7.9. Pareto-optimal solutions classified correctly: solutions that in terms of design variables are identical to the ones directly computed by means of the vehicle model

Method	$PO(\%)$
Linear	66.60
Quadratic	67.60
RBFNN gaussian	73.01
RBFNN thin plate spline	74.55
MLPNN	77.10

PO is the ratio between the number of Pareto-optimal solutions obtained by means of the approximated model $\hat{f}$ and the number of Pareto-optimal solutions obtained by means of the vehicle model (expressed in percentage)

The ultimate purpose of multi-objective optimisation methods integrated by global approximation is to compute a good approximation of the Pareto-optimal set. The Pareto-optimal set has been computed for the test set $\mathcal{T}(N_T)$ by using Definition 2.7. The test set $\mathcal{T}(N_T)$ has been obtained directly by using the vehicle model. In the same way the approximated Pareto-optimal set has been obtained by using the approximated models by considering the same design variables vectors which define the test set $\mathcal{T}(N_T)$. Table 7.9 shows the comparisons. By using the MLPNN, 77.1% of the points belonging to the approximated Pareto-optimal set are the same Pareto-optimal points (in terms of design variables) found directly by using the vehicle model. This is the best performance even if the two RBFNN obtain 73.01 and 74.55%, not so far from MLPNN. The Pareto-optimal set has been computed also for a test set $\mathcal{F}(N_F)$, obtained from $\mathcal{T}(N_T)$ considering the solution that improve all the objective functions with respect to the reference vehicle ($N_F = 787$) (see Table 7.10). In this case for the MLPNN, 71.00% of the points belonging to the approximated Pareto-optimal set are coincident with the solutions

Table 7.10. Pareto-optimal solutions correctly classified on the subset of the set solutions that improve all the objective functions with respect to a reference vehicle: solutions that in terms of design variables are identical to the ones directly computed by means of the vehicle model

Method	$PO(\%)$
Linear	37.73
Quadratic	64.26
RBFNN gaussian	69.86
RBFNN thin plate spline	70.37
MLPNN	71.00

PO is the ratio between the number of Pareto-optimal solutions obtained by means of the approximated model $\hat{f}$ and the number of Pareto-optimal solutions obtained by means of the vehicle model (expressed in percentage)

obtained by using the vehicle model; in this case too this is the best performance even if the two RBFNN (69.86 and 70.37%) perform in similar way as MLPNN.

Finally, Table 7.11 shows respectively the time needed to generate the training set, the time needed to obtain the parameters of the approximation model to generate the approximated objective functions from the test set and the time needed to complete the optimisation process on a Pentium PIII 800 using a sample of 100,000 solutions. The time needed to generate the Pareto-optimal set from the test set by obtaining the objective functions directly from the vehicle model without using global approximation is more than $1 \cdot 10^7$ s. In all the cases the optimisation process obtained by using global approximation is by far cheaper in terms of computation time with respect to the optimisation process obtained without using the approximation method. The time needed to the global approximation methods is mainly due to the evaluation of the training set. For the MLPNN, the time needed for the determination of the net architecture is relevant. RBFNN can be successfully used when a trade-off between accuracy and computation time is required.

7.6 Conclusion

In order to achieve the best performances from a racing car, the contemporary tuning of tyre and suspension design variables has proved to be necessary. To optimise a racing car, the multi-objective optimisation approach has been followed (see Chap. 3). This approach requires both validated models and a well-defined experimental activity aimed to derive the design variables that influence the dynamic behaviour of the car, namely tyre characteristics and other chassis parameters.

Table 7.11. Computation time, expressed in seconds, obtained using a Pentium PIII 800 processor

Method	1 (s)	2 (s)	3 (s)	Total (s)
Linear	1.4×10^5	6	2.4×10^2	1.4×10^5
Quadratic	1.4×10^5	7.0×10^1	7.0×10^2	1.4×10^5
RBFNN Gaussian	1.4×10^5	1.9×10^4	1.3×10^3	1.6×10^5
RBFNN thin pl. spl.	1.4×10^5	2.5×10^4	1.3×10^3	1.7×10^5
MLPNN	1.4×10^5	1.5×10^4	1.7×10^3	$\simeq 2.1 \times 10^5$

(1) Time needed to generate the training set.
(2) Time needed to generate the approximation model.
(3) Time needed to generate the Pareto-optimal set using the Quasi-Monte Carlo method (100,000 evaluations). The time needed to generate the Pareto-optimal set using the quasi-Monte Carlo method without global approximation is $>10^7$ s

According to the global approximation procedure, the complex physical model of the vehicle has been substituted by an artificial neural network that is able to approximate very closely the relationships between tyre/chassis design variables and objective functions. By means of the neural network many ($>10^6$) simulations have been performed within an extremely short time (24 h). From these simulations the optimal solutions have been selected according to Pareto theory. The dynamic behaviour of a preferred optimal car has been discussed in detail. Sensible improvements of the whole objective functions describing the vehicle dynamic behaviour have been obtained for this optimised car, with respect to the reference one.

Professional drivers have tested a number of cars fitted with the optimal suspension/tyre settings. The simulation results have been confirmed by ground tests.

The presented results showed that multi-layer perceptron neural network gives the highest accuracy. A similar performance in approximating objective functions is provided by radial basis function neural network. This result seems very encouraging because the training of RBFNN require the user to set only one parameter, contrary to MLPNN which requires much expertise to set the number of hidden layers and the number of neurons in order to obtain the best global approximation performance. Obviously, the presented results are not intended to be a general comparison between the considered global approximation methods, although the testing has been performed on an actual and very complex engineering problem. The results can be reputed valid only for similar optimisation problems.

The global approximation procedure may be used to analyse a large number of optimal solutions. The approach based on the presented low discrepancy sequences allows not only to build good approximation models but also to improve the knowledge of the designer about the relationships between design variables and objective functions. From the analysis of the presented

simulations, it appears that the Pareto-optimal set can be computed adequately by using high accuracy approximators.

With reference to the design of a vehicle tyre/suspension system, the adopted procedure has proved to be reliable and effective for obtaining higher car performance reducing the time needed in expensive ground tests.

The method allowed both to synthesise and analyse the optimal solutions in order to improve not only the performances of the car under consideration but also the know-how and the skills of designers.